Supplementary Information For

Highly Stable and Conductive Microcapsules for Enhancement of Joule Heating Performance

Zhaoliang Zheng,[†] *Jidong Jin,*[‡] *Guang-Kui Xu,*[§]* *Jianli Zou,*[†] *Ulrike Wais,*[†] *Alison Beckett,*[||] *Tobias Heil,*[¶] *Sean Higgins,*[#] *Lunhui Guan,*[ς] *Ying Wang,*[§] *and Dmitry Shchukin*[†]*

[†]Stephenson Institute for Renewable Energy and Department of Chemistry, University of Liverpool, Liverpool, L69 7ZD, United Kingdom.
Email: d.shchukin@liverpool.ac.uk
[‡]Department of Electrical Engineering and Electronics, University of Liverpool, Liverpool, L69 3GJ, United Kingdom.
[§]International Center for Applied Mechanics, State Key Laboratory for Strength and Vibration of Mechanical Structures, Xi'an Jiaotong University, Xi'an, 710049, China.
Email: guangkuixu@mail.xjtu.edu.cn
[||]EM Unit, Department of Cellular & Molecular Physiology, University of Liverpool, Liverpool, L69 3BX, United Kingdom.
[¶]Nanoinvestigation Centre at Liverpool, University of Liverpool, Liverpool, L69 3GL, United Kingdom.
[#]Centre for Materials Discovery, University of Liverpool, Liverpool L69 7ZD, United Kingdom.
[ς]Fujian Institute of Research on the Structure of Matter, Chinese Academy of Sciences, Fuzhou 350002, China.

METHODS

Exfoliation of graphite into graphene oxide in aqueous solutions. Graphite flakes (Sigma-Aldrich) were oxidized using a modified Hummers' method.[1] In brief, a 9:1 mixture of concentrated H_2SO_4/H_3PO_4 (180:20 mL) was added to a mixture of graphite flakes (1.5 g, 1 wt.% equiv.) and $KMnO_4$ (9.0 g, 6 wt.% equiv.). The reaction was then heated to 50 °C and stirred for another 12 h. Afterwards, the mixture was cooled to room temperature and poured onto ice (200 mL) with 30% H_2O_2 (1.5 mL). The mixture was then vacuum filtrated. The remaining solid material was washed in succession with 100 mL of water, 100 mL of 30% HCl, and 100 mL of ethanol (2×), followed by vacuum filtration. The material remaining was coagulated with 100 mL of ether and the resulting suspension was filtered over a PTFE membrane with a 0.45 μm pore size. The solid obtained on the filter was vacuum-dried overnight at room temperature, resulting in 2 g of the product. An aqueous solution with concentration of 2 mg/mL was prepared.

Acidic functionalization of CNTs. Multi-wall CNTs (MWCNT, diameter: 20–40 nm, length: 5-15 μm, purity: 95–98%) prepared by the catalytic decomposition of methane (CH_4) were purchased from the Shenzhen Nanotechnologies Ltd. Co (China). According to previous report,[2] 3 g of the MWNTs are refluxed in 90 mL of HNO_3 (65 wt.%) at 140 °C for 12 h. The acid treated MWCNTs were rinsed with DI water until a neutral pH value is reached. After vacuum drying, an aqueous solution with concentration of 2 mg/mL was prepared.

Formation of C22@GO-CNT/GO composites. The planar C22@GO-CNT/GO composites were prepared by filtrating aqueous solution with different C22@GO-CNT concentration,

ranging from 0, 25, 50, 75 and 100%. Cellulose acetate membrane filters (OE67, 0.45 μm, Whatman™) were used in filtration.

Reduction of C22@GO-CNT/GO composites. Samples were immersed in an HI solution (55% in DI) and kept at room temperature for one day. After that, it was rinsed with water until no more brown colour could be seen. The planar composites were further dried in vacuum.

Transmission Electron Microscopy observation of GO-CNT hybrids. GO-CNT hybrids were investigated using a JEOL 2100FCs with a Schottky Field Emission Gun transmission electron microscope (200 kV accelerating voltage). Samples were collected on carbon-coated copper grids (Holey Carbon Film, 300 mesh Cu, Agar Scientific, Essex, UK) after being briefly dispersed ultrasonically in water.

Ultramicrotomy and TEM observation of microcapsules. Samples were embedded in LR White Acrylic Resin (TAAB L012/L010) and cold cured in either an embedding mould or gelatine capsules. Both were placed on ice to disperse the heat produced by the exothermic reaction.

Ultrathin section (70-80nm) were cut on a Leica UC6 Ultramicrotome and collected on glow discharged, formvar coated copper grids. Grids were post stained for 5 minutes with both 4% uranyl acetate and Reynolds lead citrate before viewing at 120KV in a FEI Tecnai G^2 Spirit.

Scanning electron microscopy. SEM analysis was performed using a JSM-7001F Scanning Electron Microscope from JEOL. The samples were coated with chromium for 60 s and examined. The microcapsules were observed directly after the drop of reaction mixture was dried

on an aluminium SEM stub overnight at room temperature. The cross section of 2D C22@GO-CNT/GO composites were observed when the samples were stabilized vertically on a sample holder.

To examine the configuration of CNTs inside C22@GO-CNT microcapsules, the as-prepared C22@GO-CNT microcapsules were first dried on a glass plate, which was followed by immersion into hexane overnight. After vacuum drying, a tap was utilized to peel the upside of the capsules.

Hot stage-digital camera technology. The shape stability was investigated by recording the states of the samples at different circumambient temperatures with digital images. Samples were placed on a copper stage equipped with a thermocouple by which the temperature increased at the rate of 5 °C /min from room temperature to 50 °C. (5 °C/min to 50 °C), revealing no detectable leakage during phase transition and melting state of docosane

Raman spectroscopy. Raman spectra were measured by the Renishaw InVia Raman microscope with a 532 nm laser and a 50× objective lens. The spot is 1.1 μm. The incident laser power is 1 mW (0.5%) and the exposure time is 20 s.

Thermogravimetric analysis (TG) and derivative thermogravimetric (DTG) analyses. This technique was used to investigate the docosane mass percentages and thermal stability of the as-prepared capsules using a microbalance model STA PT1000 from Linseis. Before measurement, microcapsules were cryogenically frozen by submersion in liquid N_2 before being freeze-dried in a Virtis AdVantage freeze drier (duration: 48 h, shelf temperature: −90 °C). Then, the samples were heated at 5 °C/min from 25 °C to 800 °C in a stream of N_2.

Differential Scanning Calorimetry (DSC). The phase change behaviour was evaluated using a calorimeter model Q20 from TA Instruments. Normally, samples were heated and cooled at 5 °C/min from 0 °C to 80 °C in a sealed nitrogen atmosphere at a flow rate of 60 mL/min. For fast thermal scan, the heat and cool rate could be up to 10 °C/min. Indium was used as a reference for calibration of the DSC. The temperature accuracy was ±0.1 °C and heat flow repeatability was 0.2 mW. 5–6 mg of samples was sealed in an aluminium pan.

Light the LED lamp. The lamp can be lighted under forward bias (around 1.8 V) circuit.

MD Simulations. The molecular dynamics (MD) simulations are performed to investigate the interactions between graphene oxide (GO) and carbon nanotube (CNT). The simplistically small graphene with several Hydroxyl groups is established by using the Material Studio 8.0, and the geometric parameters are fully optimized by the density functional theory within the generalized-gradient approximation (GGA) with the Perdew–Burke–Ernzerhof (PBE) function.[3] The optimized Hydroxyl groups are ported to the larger graphene with dimensions of 20 nm in length and 12 nm in width, while the CNT of 20 nm in length and 0.7 nm in radius is placed over the GO layer at an appropriate distance. Then, the GO-CNT system is relaxed by carrying out the Large-scale Atomic/Molecular Massively Parallel Simulator (LAMMPS). In MD simulations, the REAX potential function[4] is used to describe the interaction between atoms, and the NVT ensemble is chosen to keep the temperature of the initial structure at 500 K.

Supporting Note 1

The completely horizontal adherence via π - π interaction[5,6] induces an interaction energy is $E_{\mathrm{CNT-GO}} = \gamma_{\mathrm{CNT-GO}} S_{\mathrm{CNT-GO}}$ where $\gamma_{\mathrm{CNT-GO}}$ and $S_{\mathrm{CNT-GO}}$ denote the interface strength and the effective contact area between CNTs and GO sheets, respectively. A perfect embedment results in the interaction energy between CNT and docosane is $E_{\mathrm{CNT-C22}} = \gamma_{\mathrm{CNT-C22}} S_{\mathrm{CNT-C22}}$. Here we know $S_{\mathrm{CNT-GO}} = wL$ with w being the effective contact width and L being the length of CNTs; while, $S_{\mathrm{CNT-C22}} = 2\pi RL$ with R being the radius of CNT. For CNTs the width w should be much smaller than $2\pi R$, and thus, the contact area $S_{\mathrm{CNT-GO}}$ is smaller than $S_{\mathrm{CNT-PCM}}$. However, $\gamma_{\mathrm{CNT-GO}}$ (around ca. -500 kJ/mol[7]) was reported to be two orders of magnitude larger than $\gamma_{\mathrm{CNT-PCM}}$ (-6.07 KJ/mol[8]). The preferable configuration for CNTs inside microcapsules is not clear yet based on the recent data. But it is straight-forward to speculate that short CNTs can completely adhere on GO layer because $E_{\mathrm{CNT-GO}}$ is taking more dominant effect; and yet the effect of L will become obvious in the case of long CNTs, resulting in the configuration of partially adhering on GO layer and partially extending into the interior.

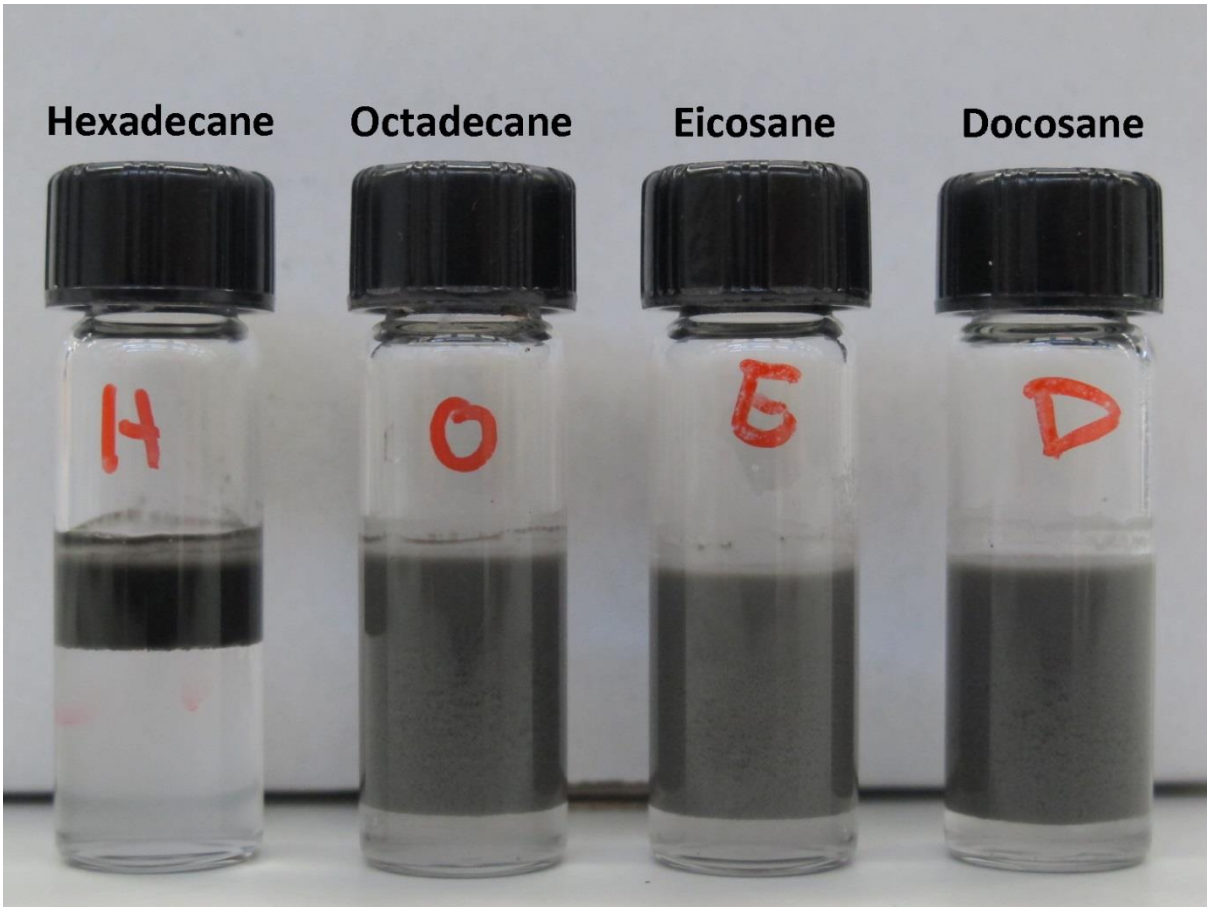

Figure S1. The emulsions are stable for long-chain alkanes. The microemulsification process was widely applicable to different alkanes. The as-prepared micoremulsions were stable beyond two months' storage.

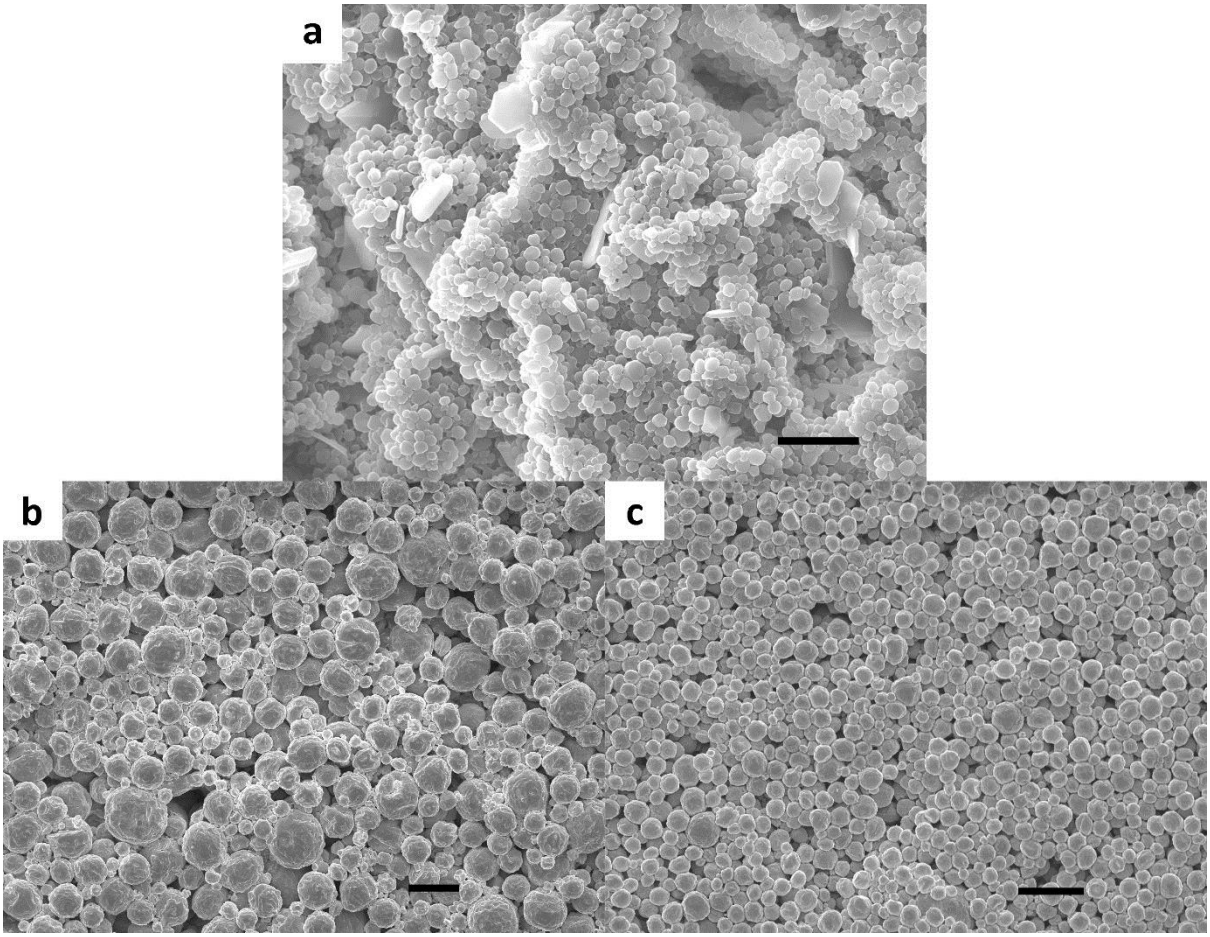

Figure S2. SEM images of as-prepared C22@GO-CNT, C22@GO and C22@-CNT microcapsules. Sizes of C22@GO-CNT (500/10/0.2), C22@GO (500/10/0) and C22@CNT (500/0/10) are 1.3 ± 0.3 μm, 6.9 ± 1.9 μm and 2.6 ± 0.6 μm, respectively. Scale bar: 10 μm.

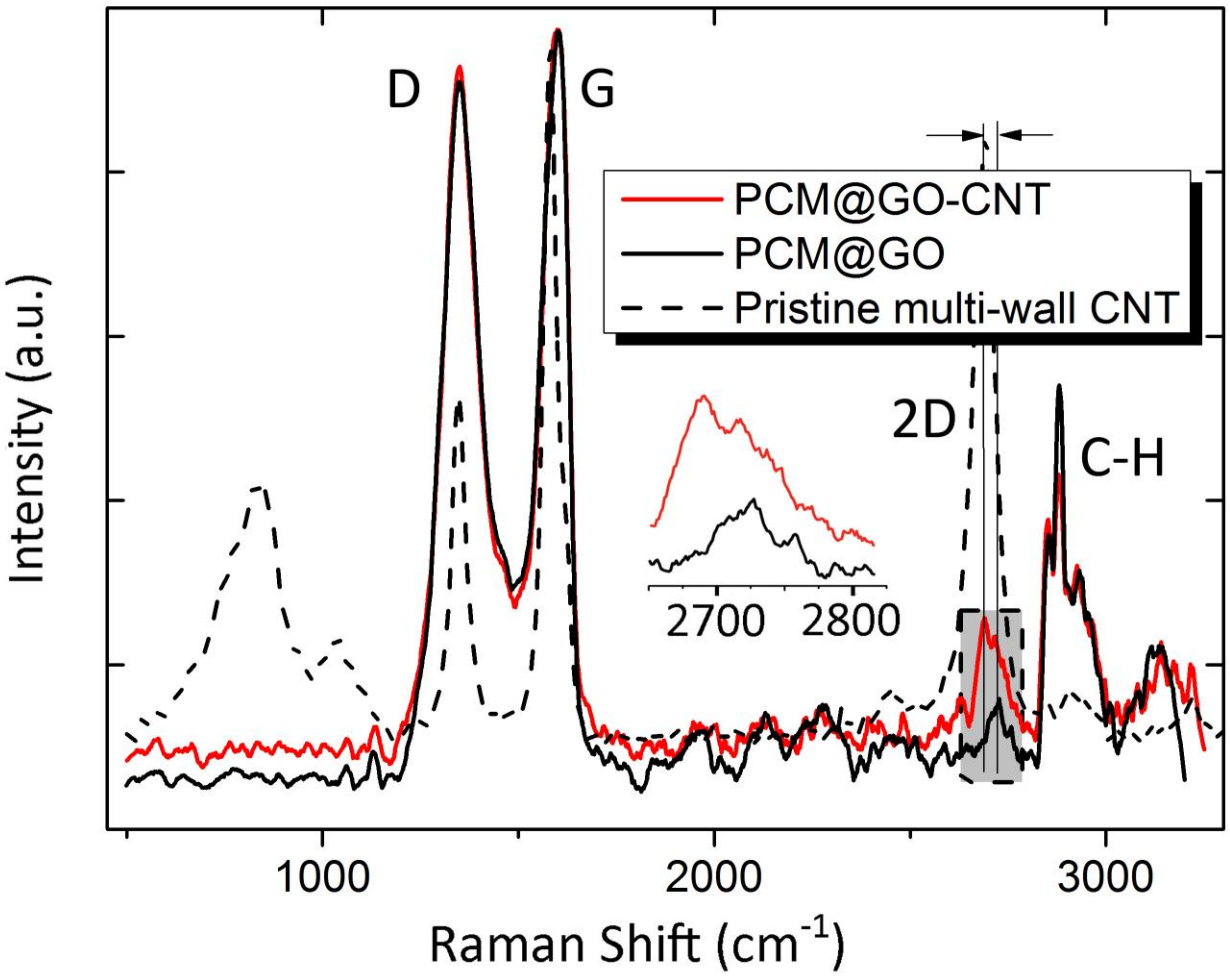

Figure S3. The Raman spectrum of pristine CNTs, C22@GO and C22@GO-CNT. For C22@GO and C22@GO-CNT, the spectrum contain almost-overlapping D-band (~1350 cm^{-1}, disorder in the graphene oxide lattice), the G-band (~1600 cm^{-1}, phonon scattering of the graphitic structure),[9] and C-H stretching region (between 2800 and 3000 cm^{-1}).[10] They differentiate from each other at the 2D-band (grey zone) due to the introduction of CNTs. The Raman spectrum of pristine CNTs is different with a lower D/G intensity ratio, narrowed and left-shifted D- and G-bands, and most notably, a much stronger 2D-band centred at 2700 cm^{-1} (double resonance process among stacked CNT walls).

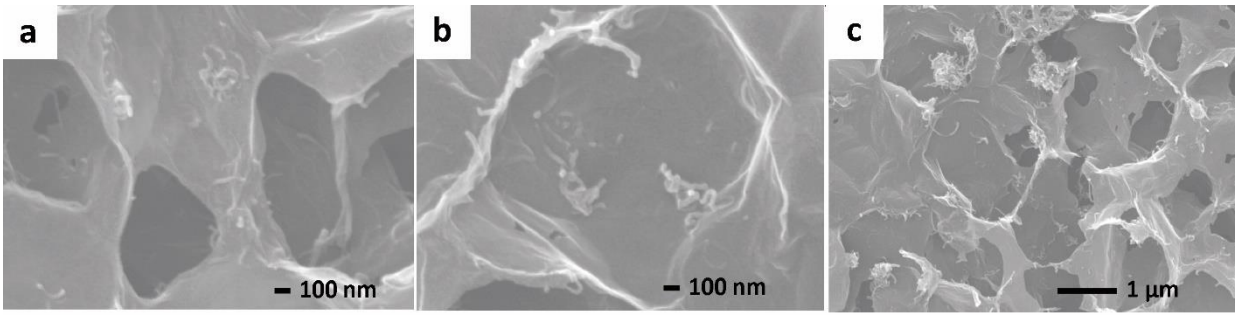

Figure 4. Direct observation of CNT configurations. SEM was utilized to confirm the multiform of CNTs inside C22@GO-CNT microcapsules. CNTs are found exclusively in void spaces of original encapsulated docosane after removal of the encapsulated docosane and the topside of some capsules.

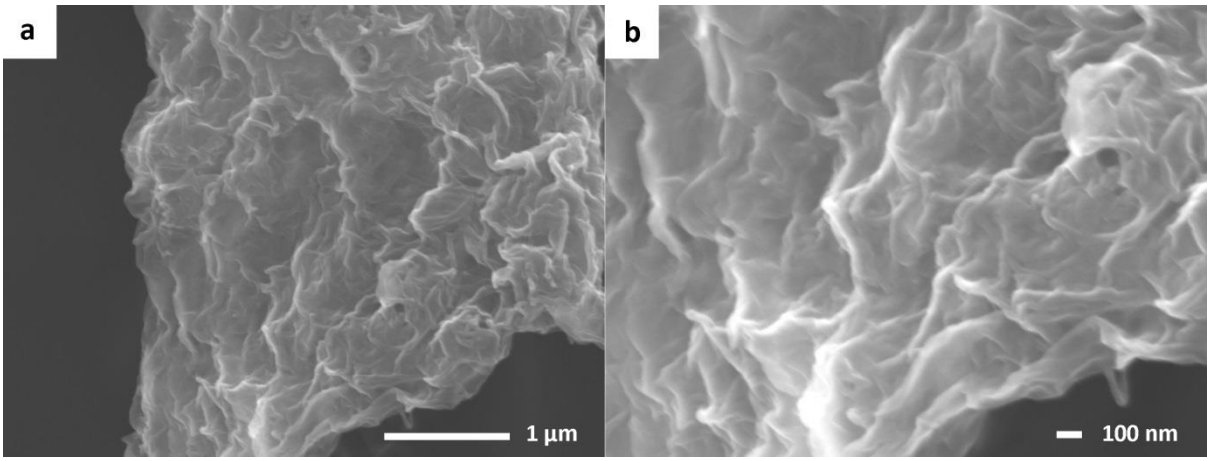

Figure S5. SEM images of the GO-CNT hybrids in magnification of (a) ×25,000 and (b) ×50,000.

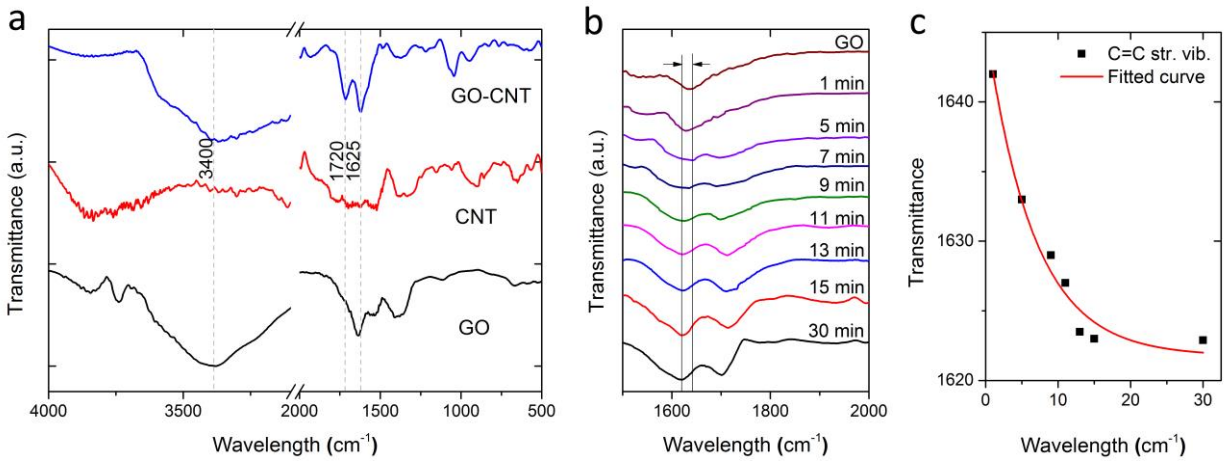

Figure S6. Hybrid structure between GO and CNT are formed. (a) The infrared (IR) absorbance spectrums show a peak representing GO C=C stretching vibration blue-shifts from 1642 cm^{-1} to 1623 cm^{-1}. Besides, more carboxyl groups were generated under ultrasound. It is because C=O stretching vibration (at 1720 cm^{-1}) of GO-CNT hybrids becomes stronger than that of the GO sample. The peak at 3400 cm^{-1} represents the O-H stretching vibration mode. (b) The blue shift of C=C stretching vibration with time (0 – 30 min) is highlighted with IR spectrums at the wavelength range from 1500 to 2000 cm^{-1}. (c) The shift with time can be fitted using first-order kinetics, indicating that the assembly reaches saturate state at the 15^{th} min.

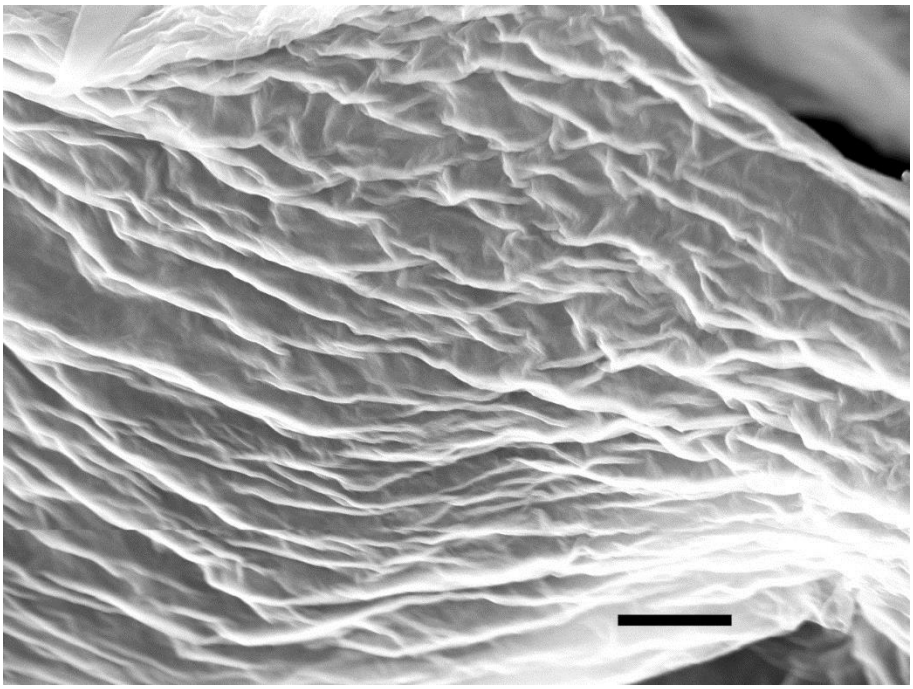

Figure S7. SEM image of GO sheets after ultrasound treatment. Scale bar: 1 μm.

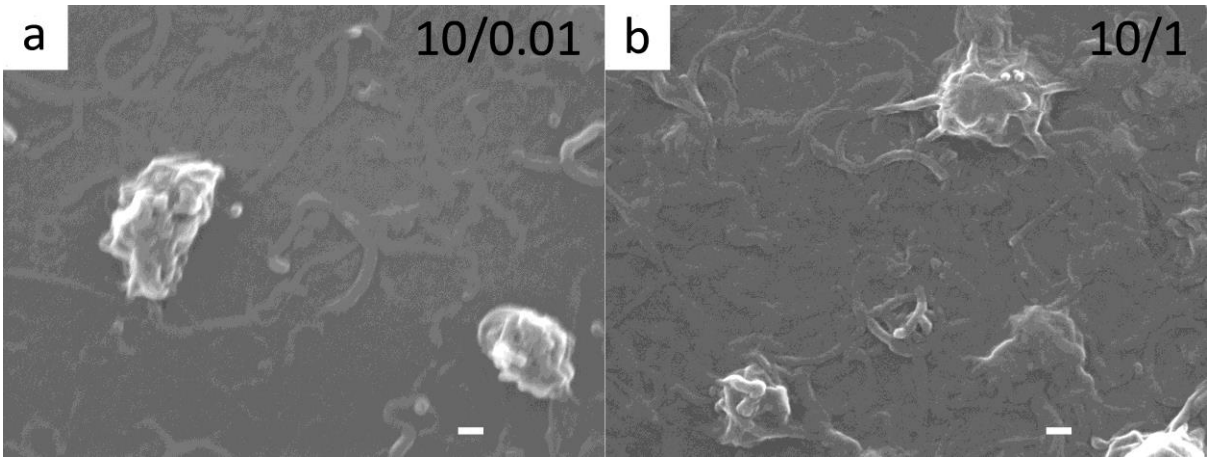

Figure S8. SEM images of GO-CNT hybrids formed with GO/CNT weight ratio of (a) 10/0.01 and (b) 10/1.

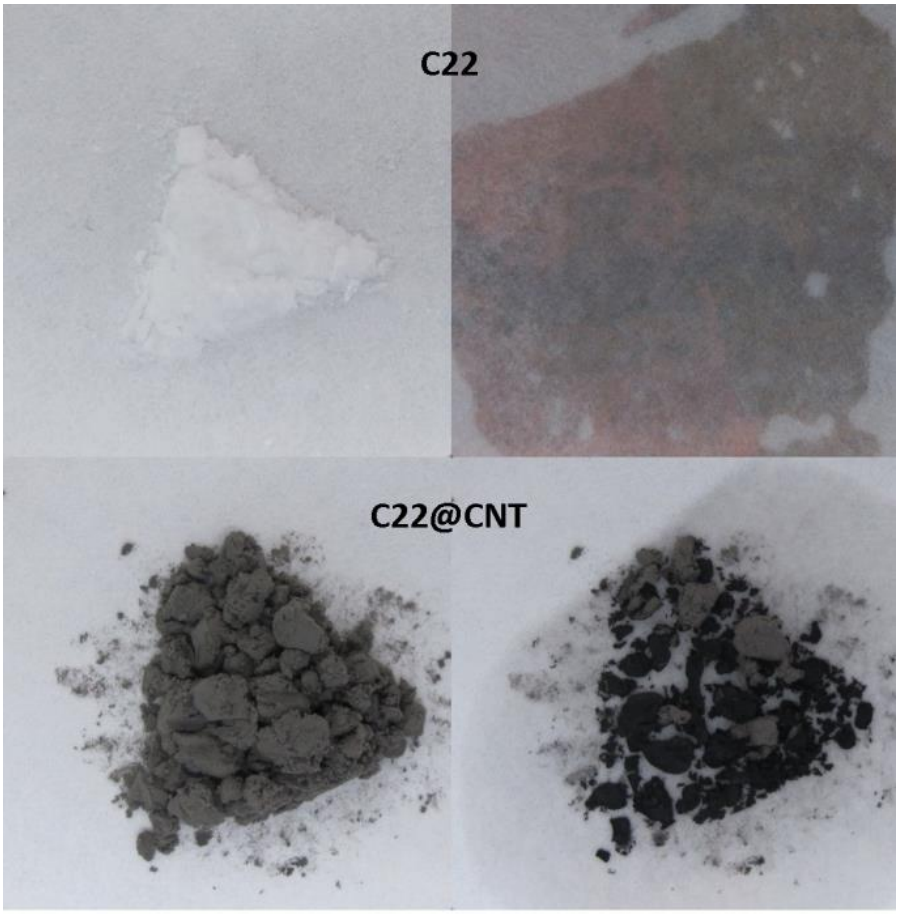

Figure S9. The shape-stability of C22 and C22@ CNT. After freeze drying, the form-stable properties of C22 and C22@CNT were evaluated using hot stage-digital camera technology. The shape changes at around 50 ^{0}C are shown.

Figure S10. The microemulsions are pH resistant. The as-prepared C22@GO-CNT emulsions (left) were stable even the pH was tuned up to 7. Contrarily, C22@GO (right) exhibited server docosane leakage in the same condition, which indicated that the GO shells were further strengthened by CNTs. GO is sensitive to pH change because of hydroxyl, carbonyl and epoxy groups on the basal plane and carboxylic groups mainly at the edges of GO sheets. Increasing hydrophilicity of GO by rising pH value can usually weaken the stability of emulsions stabilized by GO.[11-13]

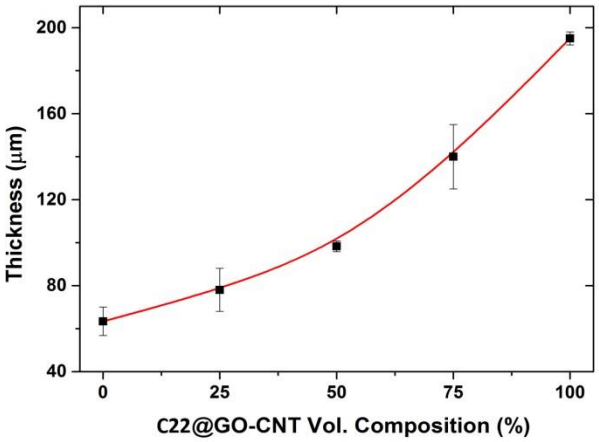

Figure S11. Thickness of C22@GO-CNT composites increases with C22@GO-CNT volume concentration. The averaged thickness of the composites as a function of C22@GO-CNT microcapsule concentration. The individual thickness ranges from 63.4 to 195 μm by adjusting the volume concentration of C22@GO-CNT microcapsules from 0 to 100%.

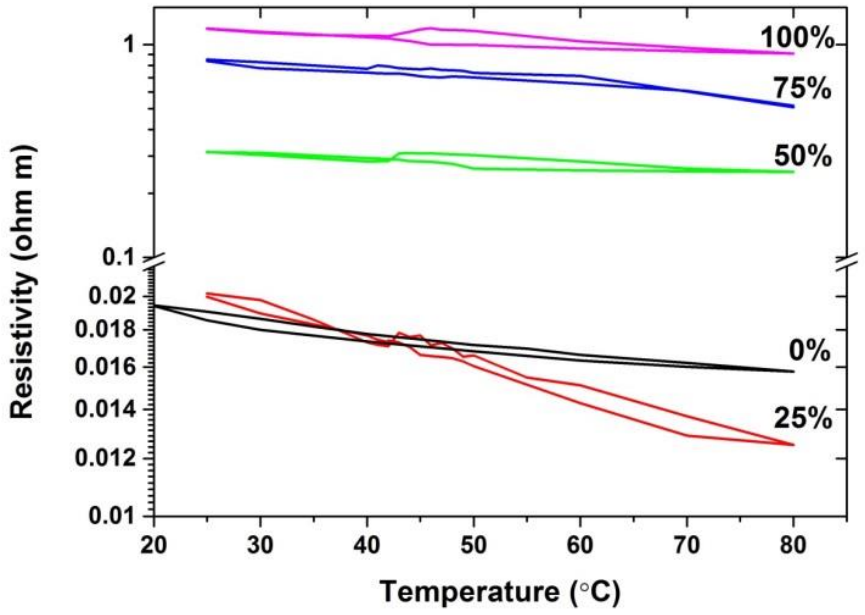

Figure S12. Electrical resistivity curve of rC22@GO-CNT/GO composites. rC22@GO-CNT/GO composites made up with different concentration of C22@GO-CNT (0, 25%, 50%, 75% and 100%) were tested for with a four-point probe set-up. The temperature of stage underneath was controlled by a digital thermocouple.

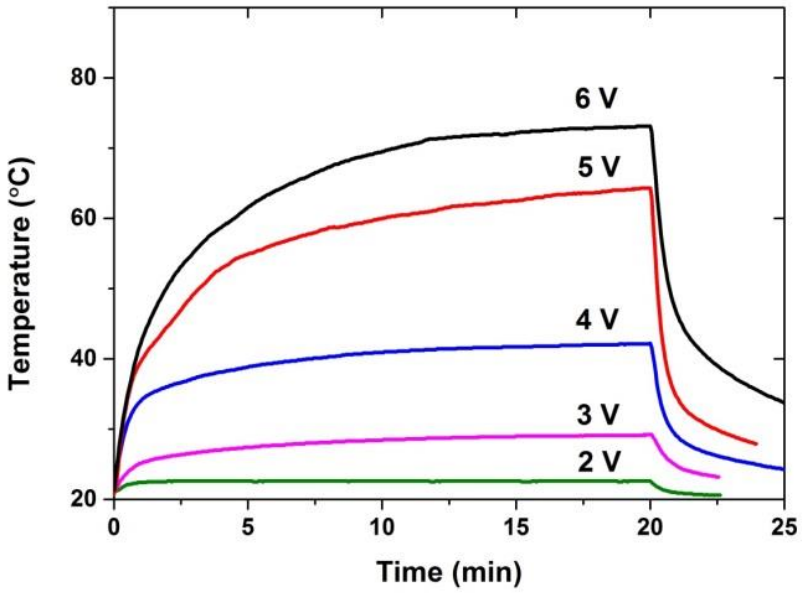

Figure S13. Electrothermal performance of neat rGO Joule heater. Temperature evolution curves of neat rGO Joule heater under constant voltages of 2, 3, 4, 5 and 6 V. Each potential was applied for about 20 min and then removed.

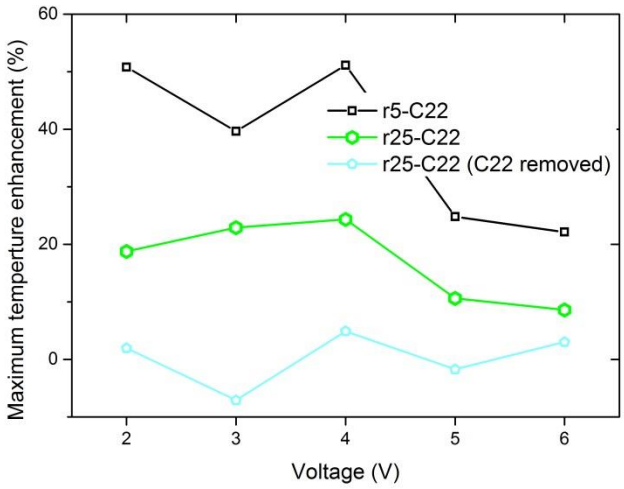

Figure S14. Enhanced Electrothermal performance. The maximum temperature enhancements as compared with neat rGO Joule heater are shown. r5-C22@GO-CNT/GO, r25-C22@GO-CNT/GO and r25-C22@GO-CNT/GO without C22 were investigated under constant voltages of 2, 3, 4, 5 and 6 V.

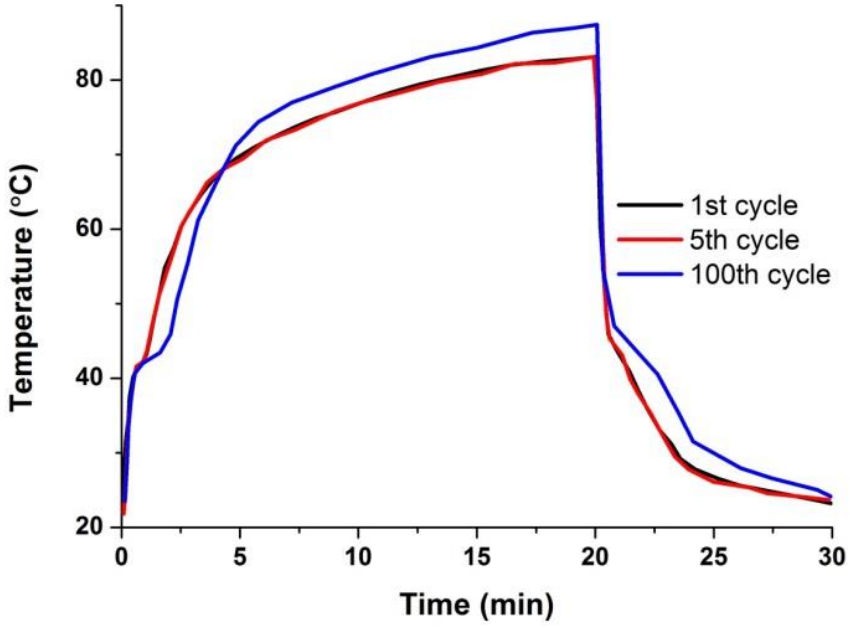

Figure S15. Stable electrothermal performance of r25-C22@GO-CNT composite. A collection of temperature evolution curves of r25-C22@GO-CNT/GO composite under 6 V repeated for 100 cycles.

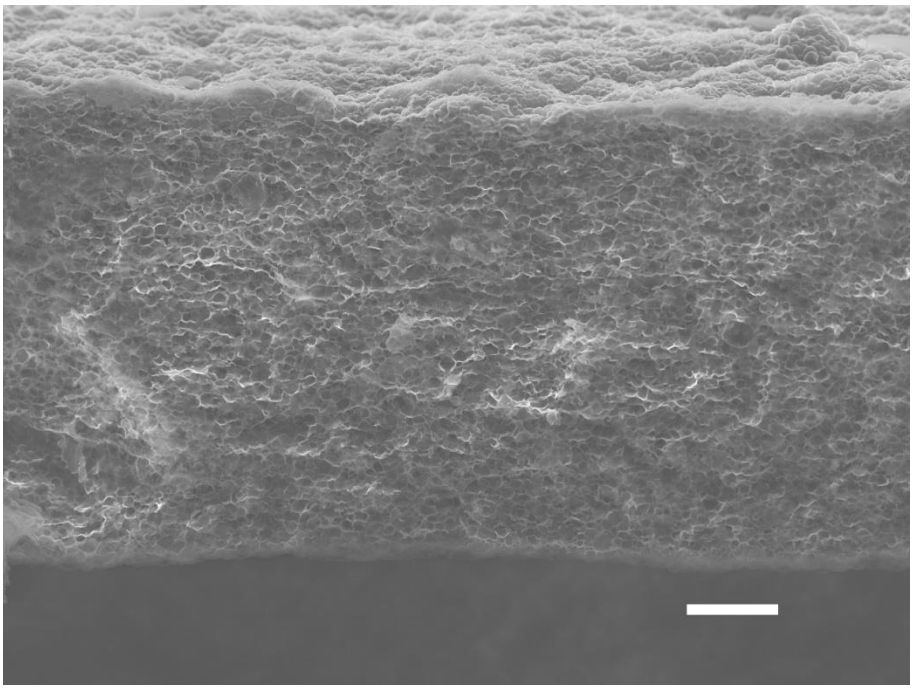

Figure S16. SEM image of the sample without docosane. Docosane was removed from r25-C22@GO-CNT/GO composite by hexane. Scale bar: 10 μm.

REFERENCES

(1) Marcano, D. C.; Kosynkin, D. V.; Berlin, J. M.; Sinitskii, A.; Sun, Z. Z.; Slesarev, A.; Alemany, L. B.; Lu, W.; Tour, J. M.,Improved Synthesis of Graphene Oxide. *Acs Nano* **2010**, *4*, 4806-4814.

(2) Li, J. X., Wen, W. W., Zou, M. Z., Guan, L. H.; Huang, Z. G. MWNT-Supported Bifunctional Catalyst of *Beta*-FeOOH Nanospindles for Enhanced Rechargeable Li-O-2 Batteries. *J. Alloy Compd.* **2015**, *639*, 428-434.

(3) Perdew, J. P.; Burke, K.; Ernzerhof, M. Generalized Gradient Approximation Made Simple. *Phys. Rev. Lett.* **1996**, *77*, 3865-3868.

(4) Nielson, K. D.; van Duin, A. C. T.; Oxgaard, J.; Deng, W. Q.; Goddard, W. A. Development of the ReaxFF Reactive Force Field for Describing Transition Metal Catalyzed Reactions, with Application to the Initial Stages of the Catalytic Formation of Carbon Nanotubes. *J. Phys. Chem. A* **2005**, *109*, 493-499.

(5) Guldi, D. M.; Rahman, G. M. A.; Jux, N.; Balbinot, D.; Hartnagel, U.; Tagmatarchis, N.; Prato, M. Functional Single-Wall Carbon Nanotube Nanohybrids Associating SWNTs with Water-Soluble Enzyme Model Systems. *J. Am. Chem. Soc.* **2005**, *127*, 9830-9838.

(6) Tung, V. C.; Huang, J.-H.; Tevis, I.; Kim, F.; Kim, J.; Chu, C.-W.; Stupp, S. I.; Huang, J. Surfactant-Free Water-Processable Photoconductive All-Carbon Composite. *J. Am. Chem. Soc.* **2011**, *133*, 4940-4947.

(7) Seydou, M.; Marsaudon, S.; Buchoux, J.; Aimé, J. P.; Bonnot, A. M. Molecular Mechanics Investigations of Carbon Nanotube and Graphene Sheet Interaction. *Phys. Rev. B* **2009**, *80*, 245421.

(8) Tsuzuki, S.; Honda, K.; Uchimaru, T.; Mikami, M.; Tanabe, K. Origin of the Attraction and Directionality of the NH/π Interaction: Comparison with OH/π and CH/π Interactions. *J. Am. Chem. Soc.* **2000**, *122*, 11450-11458.

(9) Stankovich, S.; Dikin, D. A.; Piner, R. D.; Kohlhaas, K. A.; Kleinhammes, A.; Jia, Y.; Wu, Y.; Nguyen, S. T.; Ruoff, R. S. Synthesis of Graphene-based Nanosheets via Chemical Reduction of Exfoliated Graphite Oxide. *Carbon* **2007**, *45*, 1558-1565.

(10) Camp Jr, C. H.; Cicerone, M. T. Chemically Sensitive Bioimaging with Coherent Raman Scattering. *Nat. Photon.* **2015**, *9*, 295-305.

(11) Kim, J.; Cote, L. J.; Kim, F.; Yuan, W.; Shull, K. R.; Huang, J. Graphene Oxide Sheets at Interfaces. *J. Am. Chem. Soc.* **2010**, *132*, 8180-8186.

(12) Zhang, Y.; Zheng, X. H.; Wang, H. T.; Du, Q. G. Encapsulated Phase Change Materials Stabilized by Modified Graphene Oxide. *J. Mater. Chem. A* **2014**, *2*, 5304-5314.

(13) Song, X. H.; Yang, Y. F.; Liu, J. C.; Zhao, H. Y. PS Colloidal Particles Stabilized by Graphene Oxide. *Langmuir* **2011**, *27*, 1186-1191.